



Electronic Research Archive of Blekinge Institute of Technology
<http://www.bth.se/fou/>

This is an author produced version of a paper published in IEEE
TRANSACTIONS ON AEROSPACE AND ELECTRONIC
SYSTEMS. This paper has been peer-reviewed but may not include
the final publisher proof-corrections or journal pagination.

Citation for the published paper:

Mats I. Pettersson

IEEE TRANSACTIONS ON AEROSPACE AND ELECTRONIC
SYSTEMS, Volume 40, Issue 3, Year 2004, pages 780-796

Access to the published version may
require subscription.

Published with permission from:
IEEE

Detection of moving targets in wide band SAR

Mats I. Pettersson

Abstract— A likelihood ratio is proposed for moving target detection in a wide band (WB) SAR system. For this paper, WB is defined as any systems having a large fractional bandwidth, i.e. an ultra wide frequency band combined with a wide antenna beam. The developed method combines time domain fast backprojection SAR processing methods with moving target detection using space-time processing. The proposed method reduces computational load when sets of relative speeds can be tested using the same clutter suppressed sub-aperture beams. The proposed method is tested on narrow band radar data.

I. INTRODUCTION

This paper describes a technique for detecting moving targets in a WB SAR system. Work on a Fourier-based WB SAR moving target detection technique has been published by Soumekh [1]. The approach presented here differs from Soumekh's work in two ways. First, our approach puts the moving target detection into the image formation process. Second, the image formation process is accomplished using a fast backprojection based approach. The goal of our approach is to both provide the extreme motion compensation needed in a WB SAR system and reduce the computational load. These benefits will occur in both processing stationary targets and focusing moving targets at different relative speeds [2].

Focusing a moving target in WB SAR is a difficult problem. In a WB SAR system, the integration time is long and thus the moving target may perform non-linear motions and rotations during the integration time. In this paper we consider only targets that perform linear motion over the integration interval. Still, the results demonstrated in this paper can be applied to any target over pieces of the aperture where the target motion can be approximated as linear.

Mats I. Pettersson
Division of Sensor Technology
Department of Radar Systems
Swedish Defence Research Agency
P.O. Box 1165
SE-581 11 Linköping
Sweden

E-mail: matsp@foi.se
Telephone: +46 13 378043
Fax: +46 13 378100

While Fourier-based image formation approaches provide good image quality for non-WB SAR systems, they often fail to provide adequate quality imagery in WB SAR systems, because of the long integration times needed. These large integration times impose stringent demands on the motion compensation needed to form imagery in these systems. Thus time-domain backprojection algorithms, whose origins stem from Global Backprojection (GBP) [3, 4], are better suited for forming images in a WB SAR system.

Two examples of WB SAR systems are CARABAS™ and LORA what are being developed at the Swedish Defense Research Agency (FOI) [5-7]. CARABAS is a VHF (20-90MHz) system while LORA is a dual band system with VHF (20-90MHz) and UHF (200-800MHz). LORA is the next generation of low frequency radar being developed at FOI. LORA's design is based upon CARABAS technology but extends system capabilities through both a larger bandwidth and including a UHF multi-channel antenna array. The low frequencies used by these systems, combined with their high relative resolution, provide a unique capability of detecting targets concealed in foliage [8-11]. The capabilities of the LORA system will be extended based upon the theory developed in this paper.

There is a need to detect moving targets in WB SAR. Especially there is a need to combine time domain SAR processing techniques with moving target detection. This paper addresses with this problem. In section II we discuss time domain image processing methods and how the movement of the target affects the target appearance. In section II.A we review different SAR time domain processing methods, and in section II.B we review the Local Backprojection SAR image formation algorithm. In section II.C we determine the moving target location in the SAR image. Section II.D shows how a moving target can be focused using backprojection results calculated for ground speed.

In section III we consider the antenna arrays spatial separations of the channels, and how the separation affects the location of the moving target. In section IV we show how the antenna array in WB SAR can be used to detect moving targets in strong clutter. In section IV.A we give a review in the field and in section IV.B we develop a method to detect moving targets with a WB SAR system. The method is a combination of backprojection and space-time processing, and it is derived from a likelihood ratio test. In section VI the method is tested on narrow band radar data, because there were no WB data available.

II. FAST BACKPROJECTION METHODS AND MOVING TARGETS IN A WB SAR SYSTEM

There are many different SAR image formation algorithms. The choice of algorithm is dependent on system configuration, available processing power, computer memory, and required quality of the resulting image. In WB SAR systems, it has been found that time domain backprojection algorithms have good performance [11] due to the capability to handle the extreme range

migration and motion compensation requirements associated with the wide antenna aperture.

A. Fast Backprojection Methods

Due to the extreme computational demands of the Global Backprojection (GBP) for large images, approximate yet faster time-domain algorithms have been developed. The domain of different Fast Backprojection Methods (FBPM) can be categorized based upon the number of stages used in the processing. Two-stage FBPM algorithms include Local Backprojection (LBP) [12] and the Fast Backprojection Algorithm (FBPA) [13]. Multi-stage FBPM algorithms include Quadtree Backprojection (QBP) [14], the fast backprojection method mentioned in [15] and Fast Factorized Backprojection (FFBP) [16].

For a SAR image with N aperture points and an N by N image area, the number of operations needed for GBP is proportional to N^3 while two-stage algorithms are proportional to $N^2\sqrt{N}$ and multiple-stage algorithms are proportional to $N^2 \log(N)$ [14,15,16]. Thus QBP and FFBP have the same computational load as Fourier-domain techniques. FFBP is often preferred to QBP because the resulting image quality using FFBP can be controlled using parameter fed into the algorithm.

While FFBP is often the preferred FBPM, it will not be used in this work. The motive of this paper is to provide a proof of concept of combining fast backprojection methods with moving target detection, not optimize with respect to speed. Thus the similarities in each of the fast backprojection methods allow us to select any approach in order to demonstrate our concept. For this paper, the LBP algorithm was chosen over FFBP since LBP is easier to derive mathematically.

B. The LBP

Consider Figure 1. A point target at ground position (ξ_0, η_0, ζ_0) will appear in the radar coordinate system (x, R) at different ranges given by the radar position x . Assuming a straight flight track the range migration will be a hyperbola. In the following we relate the radar coordinates to the target by the minimum range, that is when the distance between the target and the platform antenna is minimum and it is in radar coordinates given when $(x, R) = (x_0, \rho_0)$. For a non-moving target at $(\xi_0, \eta_0, 0)$ the minimum range is $\rho_0 = \sqrt{\eta_0^2 + h^2}$ and $x_0 = \xi_0$. The backprojection process places the non moving target at point (x_0, ρ_0) in the image. Assume the radar antenna moves along a linear track alongside the x-axis. The output from the radar sensor for a point target at (x, R) is given by

$$\frac{p\left(R-\sqrt{(x-x_0)^2+\rho_0^2}\right)}{(x-x_0)^2+\rho_0^2} \quad (1)$$

where $p(R)$ is the compressed pulse of a point target. From the radar output we form the signal

$$g(x,R)=\frac{p\left(R-\sqrt{(x-x_0)^2+\rho_0^2}\right)}{\sqrt{(x-x_0)^2+\rho_0^2}} \quad (2)$$

We have assumed the start-stop approximation [17] to be valid, which is reasonable in an airborne system. For GBP we define the backprojected signal $h(x,\rho)$ according to

$$h(x,\rho)=\int_{-\infty}^{\infty} g\left(x',\sqrt{(x'-x)^2+\rho^2}\right) dx' \quad (3)$$

This is a SAR image found by solving the backprojection signal (3) for each image point (x,ρ) . It can be shown that the exact inversion for a point target in a system with infinite bandwidth is found after filtering $h(x,\rho)$ with a ramp filter in wave domain [4,16]. The filtering is simply a multiplication between the wave domain transformed backprojection signal and the wave domain ramp [16]. The ramp filter lowers the sidelobes in the WB image. The interested reader can find more details about GBP in references [3,4,12,15,16].

Consider a target response located in a sub-image with center coordinates ρ_c and x_c as seen in Figure 2. In LBP the integral (3) is solved approximately over M sub-apertures with size L_s over one sub-image. The sub-image and sub-aperture are chosen sufficiently small such that the range distance can be approximated as a linear function. The LBP at (x,ρ) , for a point target in (x_0,ρ_0) , is given by

$$h(x,\rho)=\sum_{m=1}^M \int_{\left(x_m-L_s/2\right)}^{\left(x_m+L_s/2\right)} g\left(x',R_{cm}+\frac{\left(\left(x'-x_m\right)-\left(x-x_c\right)\right)\left(x_m-x_c\right)+\left(\rho-\rho_c\right)\rho_c}{R_{cm}}\right) dx' \quad (4)$$

where $R_{cm}=\sqrt{\left(x_c-x_m\right)^2+\rho_c^2}$ and x_m is the center coordinate in each sub-aperture. In LBP the sub-images and sub-aperture size L_s are sufficiently small such that the sub-aperture integral dependence on (x,ρ) in a sub-image over a sub-aperture appears as linear

range shift in $g(\bullet, \bullet)$. If we form the local range history $r = \frac{(x-x_c)(x_c-x_m) + (\rho-\rho_c)\rho_c}{R_{cm}}$ we are able to rewrite the sub-aperture

integral to

$$y(r, m) = \int_{(x_m - l/2)}^{(x_m + l/2)} g\left(x', R_{cm} + r + \frac{x_m - x_c}{R_{cm}}(x' - x_m)\right) dx' \quad (5)$$

which is called the sub-aperture beam. Also, for a particular sub-aperture m , the sub-integral depends only upon the local range.

The LBP can then be rewritten in terms of sub-aperture beams as

$$h(x, \rho) = \sum_{m=1}^M y\left(\frac{(x-x_c)(x_c-x_m) + (\rho-\rho_c)\rho_c}{R_{cm}}, m\right) \quad (6)$$

Simulations of Eq. (4-6) are given in [2,18].

C. Displacement of moving targets in the SAR image

A moving target will be displaced and unfocused in the SAR image as shown in reference [19] and in Figure 3. The location where the moving target will appear in the SAR image will be associated with the radar coordinates of minimum range (x_0, R) where $R = \rho_0$ [6,7]. As in [1] we change the image coordinate system so that the moving target is stationary resulting in the transformed platform velocity being the relative speed between the platform and the target velocities. To ease both the image formation process and detection, we chose the moving target parameterization to be connected to the minimum range in the radar coordinates rather than the selected origin of the coordinate system as in [1]. Because the range history is the same in all coordinate systems in Figure 1, the displacement in a WB SAR system can be found from the distance relation between image coordinates and ground coordinates. This relationship can be written as

$$\sqrt{\gamma^2(x(t) - x_0)^2 + \rho_0^2} = \sqrt{(x(t) - \xi(t))^2 + \eta^2(t) + h^2} \quad (7)$$

Here, γ is the relative speed, ξ and η are ground coordinates of the moving target, and h is the flight altitude. We assume linear motion of the platform, $x(t) = v_p t$, and of the moving target position $\xi(t) = v_\xi(t - t_0) + \xi_0$, $\eta(t) = v_\eta(t - t_0) + \eta_0$. The time t_0 is the time when the minimum range occurs. The moving target will be located at $(\xi_0, \eta_0, 0)$ when the antenna is at the minimum range

position x_0 . All coordinates x_0 , ξ_0 , η_0 and the time t_0 are then connected to the minimum range ρ_0 , and they can easily be found for any linear motion. Combining the distance relation in (7) with the linear motion assumption gives

$$\gamma^2 = \frac{(v_p - v_\xi)^2 + v_\eta^2}{v_p^2} \quad (8)$$

$$x_0 = \xi_0 - \frac{v_\eta}{v_p - v_\xi} \eta_0 \quad (9)$$

$$\rho_0 = \sqrt{\eta_0^2 \left(1 + \left(\frac{v_\eta}{v_p - v_\xi} \right)^2 \right) + h^2} \quad (10)$$

D. Focusing moving targets

To focus a moving target, the relative speed of that target must be taken into account in the SAR image formation process [6,19]. To apply LBP we must re-compute the sub-aperture beams and the image formation. To avoid this we propose a method to focus SAR images at γ using sub-aperture beams processed for ground speed, i.e. $\gamma=1$.

In LBP, equation (6), we sum sub-aperture beams over the hyperbola in (x_0, ρ_0) , as seen in Figure 4. If the target is moving we can still find the moving target hyperbola in the sub-aperture beams processed for $\gamma=1$. However, this requires distance compensation. In addition, if the target moves fast enough, a sub-image shift will occur between adjacent sub-images. An expression for this change in target position will now be developed.

Assume a moving target with minimum range ρ_0 at x_0 , as shown in Figure 4. To find the sub-image and range shift at x_m , we compute a point (x_0', ρ_0') , chosen such that the sub-aperture beam over this virtual non-moving target is the same as the moving target at (x_0, ρ_0) . Equating the range and range-derivative for the moving and virtual non-moving target gives

$$\sqrt{\gamma^2 (x_m - x_0)^2 + \rho_0^2} = \sqrt{(x_m - x_0')^2 + \rho_0'^2} \quad (11)$$

$$(x_m - x_0') = \gamma^2 (x_m - x_0) \quad (12)$$

Solving (11) and (12) gives x_0' and ρ_0' as functions of x_m , x_0 , ρ_0 and γ . The distance shift for a sub-aperture beam is given by

$$\Delta r_m = \sqrt{(x_m - x_0)^2 + \rho_0^2} - \sqrt{(x_m - x'_0)^2 + \rho_0'^2} \quad (13)$$

For moving targets with high speed and long integration time, Δr_m will change sufficiently such that the point (x'_0, ρ_0') moves from one sub-image to a neighboring sub-image. A sub-image shift occurs when this happens.

III. FAST BACKPROJECTION AND MOVING TARGETS IN A WB SAR SYSTEM WITH AN ANTENNA ARRAY

To detect a moving target an antenna array often used. This section describes how the antenna channel's locations affects the results derived in section II. In this article we propose an along track array similar to the antenna developed for LORA, Figure 5. Because there will be bistatic measurements between the transmitting antenna and the receiving antennas we define an effective antenna phase center. The effective antenna center approximates the bistatic wave from two displaced antennas as a monostatic wave from one antenna located in the middle of the transmitting and receiving antenna. How this approximation affects SAR processing and moving target detection is given in [1, 33]. Also the antenna configuration has a total of L channels and the separation between the first effective antenna center to the effective antenna center of channel l is d_l .

In section II.B the LBP was derived for one antenna channel. If we add more channels in an antenna array we have to take into consideration the different locations of the channels phase center. LBP can easily handle the bistatic wave originated in the array antenna, so in the processing there is no need to compensate the bistatic wave according to [1, 33]. The sub-aperture given for channel l in (5) is given by

$$y_l(r, m) = \int_{(x_m - L/2 + d_l)}^{(x_m + L/2 + d_l)} g_l \left(x', R_{cm} + r + \frac{x_m - x_c}{R_{cm}} (x' - x_m) \right) dx' \quad (14)$$

for each of the L channels in the radar system. The LBP can then be rewritten in terms of sub-aperture beams for channel l as

$$h_l(x, \rho) = \sum_{m=1}^M y_l \left(\frac{(x - x_c)(x - x_m) + (\rho - \rho_c)\rho_c}{R_{cm}}, m \right) \quad (15)$$

In section II.C we gave the displacement of the moving target in one antenna channel in equations (8-10). In an antenna array the moving target will change its position between the channels, due to the connection between space and time associated with a moving platform. We now investigate how the moving target changes its location in the other antenna channels. The amount of change by the target in each channel is given by the time difference when the minimum range occurs in the spatially separated

antenna channels. If the distance between the effective antenna phase center for channel l to the first antenna channel is d_l , the separation time Δt_l is found from (7) to be

$$\Delta t_l = \frac{d_l(v_p - v_\xi)}{(v_\xi - v_p)^2 + v_\eta^2} \quad (16)$$

For stationary targets, the time difference between the channels will be the time it takes for the platform to move from the two effective antenna centers.

From the separation time, the moving target minimum range can be found for each channel by using (8-10). The point where the minimum range occur in radar coordinates is separated for each channel to first channel by

$$\Delta x_{0l} = \frac{(v_p - v_\xi)}{v_p \gamma^2} d_l \quad (17)$$

For a stationary target (17) gives the distance d_l between the effective antenna centers which is expected. The minimum range will in each channel be separated by

$$\Delta \rho_{0l} = \sqrt{\rho_0^2 + \frac{2\eta_0 d_l v_\eta}{(v_p - v_\xi)} + \frac{d_l^2 v_\eta^2}{(v_p - v_\xi)^2 + v_\eta^2}} - \rho_0 \approx \frac{\eta_0 d_l v_\eta}{\rho_0 (v_p - v_\xi)} \quad (18)$$

where the approximation is valid when $d_l \ll 2\eta_0$ and $|2d_l v_\eta| \ll |\rho_0 (v_p - v_\xi)|$ which is true for almost all SAR radar cases with a fast platform and a target moving on ground. From the minimum range in the radar coordinate system it is easy to find target positions using the image coordinate system given by the first channel $(\gamma' x_0, \rho_0)$, where γ' is the used processing speed in image formation. However, in the other channels the SAR images are considering the spatial separation of the channels so the SAR image appearance will be $(\gamma'(x_0 + \Delta x_{0l} - d_l), \rho_0 + \Delta \rho_{0l})$ and for stationary target $\gamma=1$ processed at ground speed $\gamma'=1$ the position will in all channels be (x_0, ρ_0) .

IV. MOVING TARGET DETECTION

A. Introduction to moving targets detection in SAR

Moving target detection in radar has been well studied for many years. Detection of moving targets requires maximization of the target signal compared to the clutter. To filter moving targets from strong clutter the displaced-phase-center-antenna (DPCA) method was developed [21]. This technique needs strict spatial alignment and system stability. As an extension of an adaptive antenna technique in [22] the space-time adaptive processing (STAP) approach was developed for GMTI [23]. STAP is not only adaptive but can also be used for slow moving target detection. STAP's effectiveness with GMTI is because the clutter spectrum is normally restricted to a narrow ridge in two-dimensional space-time [24,25], which is well separated from the position of moving targets.

In recent years GMTI has developed in combination with SAR. In a SAR GMTI system the moving target will not only be detected but also imaged in its surroundings. Movement of a target will have an effect on the focus of the target in the SAR image relative to its surroundings. To suppress clutter multi-channel antenna arrays can be used. An overview of SAR GMTI is given in [26]. The main detection scheme is the Likelihood Ratio Test (LRT) [27-30]. Experimental results [31-32] have confirmed that these SAR GMTI techniques are a strong tool to detect and image moving targets in its surrounding.

B. Likelihood ratio test for moving target detection in Fast Backprojection

The geometry of the SAR platform and the moving target is given in Figure 6. The speed of the target is given by the speed v_t and heading α , and we assume linear motion on a flat plane. The moving target will appear in the sub-aperture beam connected to φ and range. The true angle to the moving target is given by φ' .

In WB systems, it is a benefit to use sub-aperture beams processed for ground speed [2,18]. Sub-aperture beams allow for frequency and angle dependent mismatch in the system as well as to save processing load and reduce data complexity. This aids in the performance of moving target detection.

The illuminated area is divided into sub-images, connected to sub-apertures through sub-aperture beams $y_i(r, m)$. If a moving target is present, the sub-aperture beams consist of a moving target $z_i(r, m)$, clutter $q_i(r, m)$ and white noise independent of direction $n_i(r, m)$. The clutter and the noise are considered to be independent. The clutter is connected to the radar backscattering while the noise originates from thermal noise in the system. These two are independent. The sub-aperture beam $y_i(r, m)$ under the two hypotheses, \mathbf{H}_0 no target present and, \mathbf{H}_1 target present are

$$\mathbf{H}_0: y_l(r, m) = a_l^c(r, m) * q_l(r, m) + n_l(r, m) \quad (19)$$

$$\mathbf{H}_1: y_l(r, m) = a_l^t(r, m) * z_l(r, m) + a_l^c(r, m) * q_l(r, m) + n_l(r, m) \quad (20)$$

for the antenna channels $l = 1, \dots, L$, where $*$ is the convolution with respect to r , $a_l^c(r, m)$ is the system response to the clutter, and $a_l^t(r, m)$ is the system response to the target. Functions $a_l^c(r, m)$ and $a_l^t(r, m)$ differ, because of the different origin directions of the target and the clutter. The measurements in the radar system will be sampled signals, thus in the following we use the sampled sub-aperture beam with vector components $y_l(r_\mu, m)$, where r_μ is the sample points in local range given by $r_\mu = r_0 + \Delta r_s \mu$, where r_0 is a constant offset, Δr_s is the sampling interval, and μ is the sampling index from 0 to $N-1$.

Experience from wide band jammer suppression in the CARABAS system (which is a WB system) indicates that the moving target detection should be done in the frequency domain [20]. The wave transformed sub-aperture beams (according to r) in LBP are located in SAR image wavenumber space and seen in Figure 7. Using sub-aperture beams it is convenient to express the wavenumber vector \mathbf{k} in a polar coordinate system with radius $k = \sqrt{k_\rho^2 + k_x^2}$ and k_ϕ (the same angle as ϕ in Figure 6 in means of stationary phase [33]). In the radial direction in wave domain we have N samples, and M sub-apertures in angular direction, the index are n and m respectively.

The received signal under the two hypotheses \mathbf{H}_0 and \mathbf{H}_1 in wavenumber space are

$$\mathbf{H}_0: \tilde{y}_l(\mathbf{k}) = \tilde{a}_l^c(\mathbf{k}) \tilde{q}_l(\mathbf{k}) + \tilde{n}_l(\mathbf{k}) \quad (21)$$

$$\mathbf{H}_1: \tilde{y}_l(\mathbf{k}) = \tilde{a}_l^t(\mathbf{k}) \tilde{s}_l(\mathbf{k}) e^{j\phi(\mathbf{k})} e^{-j(r(\mathbf{k})+(l-1)\Delta(k))k} + \tilde{a}_l^c(\mathbf{k}) \tilde{q}_l(\mathbf{k}) + \tilde{n}_l(\mathbf{k}) \quad (22)$$

for $l = 1, \dots, L$ and where \mathbf{k} is the wavenumber vector dependent on the wavenumber k and sub-aperture m (dependent on Doppler angle ϕ), $\tilde{a}_l^c(\mathbf{k})$ is the wave function of the system in the clutter direction, $\tilde{a}_l^t(\mathbf{k})$ is the wave function of the system in the target direction, $\tilde{s}_l(\mathbf{k})$ is the target scattering amplitude, $\phi(\mathbf{k})$ is the phase of the target scattering, $r(\mathbf{k})$ is the local range of the target in the sub-aperture in first channel, $\Delta(k)$ denotes the movement of the target in local range between the spatial

channels and the sum $r(\mathbf{k}) + (l-1)\Delta(\mathbf{k})$ is the target local range in channel l . For simplicity, we have in the following assumed equally separated channels, with a distance d between effective antenna centers given $d_l = (l-1)d$.

The measurement vector in wavenumber space, for all L channels and all sampled wave transformed sub-aperture beams, is an $L \cdot N \cdot M$ vector

$$\tilde{\mathbf{Y}} = \begin{bmatrix} \tilde{y}_1(k_0, \varphi_1) \\ \tilde{y}_2(k_0, \varphi_1) \\ \vdots \\ \tilde{y}_L(k_0, \varphi_1) \\ \tilde{y}_1(k_1, \varphi_1) \\ \vdots \\ \tilde{y}_L(k_{N-1}, \varphi_1) \\ \vdots \\ \tilde{y}_L(k_{N-1}, \varphi_M) \end{bmatrix} = \begin{cases} \tilde{\mathbf{q}} + \tilde{\mathbf{n}} & \text{under } \mathbf{H}_0 \\ \tilde{\mathbf{A}} + \tilde{\mathbf{q}} + \tilde{\mathbf{n}} & \text{under } \mathbf{H}_1 \end{cases} \quad (23)$$

where $\tilde{\mathbf{q}}$ and $\tilde{\mathbf{n}}$ are the clutter and noise vectors, respectively. The antenna pattern in a WB SAR system is very broad and therefore the antenna changes slowly with angle. The antenna changes will probably be small between $\tilde{a}_l^c(\mathbf{k})$ and $\tilde{a}_l^c(\mathbf{k})$. In this paper we assume all antennas have the same gain in all directions and that there are no frequency dependencies in the system, i.e. $\tilde{a}_l^c(\mathbf{k}) = \tilde{a}_l^c(\mathbf{k}) = 1$. The signal vector is then given by

$$\tilde{\mathbf{A}} = \begin{bmatrix} e^{j\phi(k_0, \varphi_1)} s(k_0, \varphi_1) e^{-jk_0 r_1^t} \\ e^{j\phi(k_0, \varphi_1)} s(k_0, \varphi_1) e^{-jk_0(r_1^t + d(\cos \varphi_1 - \cos \varphi_1))} \\ \vdots \\ e^{j\phi(k_0, \varphi_1)} s(k_0, \varphi_1) e^{-jk_0(r_1^t + (L-1)d(\cos \varphi_1 - \cos \varphi_1))} \\ e^{j\phi(k_1, \varphi_1)} s(k_1, \varphi_1) e^{jk_1 r_1^t} \\ \vdots \\ e^{j\phi(k_{N-1}, \varphi_1)} s(k_{N-1}, \varphi_1) e^{-jk_{N-1}(r_1^t + (L-1)d(\cos \varphi_1 - \cos \varphi_1))} \\ \vdots \\ e^{j\phi(k_{N-1}, \varphi_M)} s(k_{N-1}, \varphi_M) e^{-jk_{N-1}(r_M^t + (L-1)d(\cos \varphi_M - \cos \varphi_M))} \end{bmatrix} \quad (24)$$

According to section II.D the moving target will perform a range history in the sub-apertures r_m^t given by minimum range and (13).

To test for the presence of a target, we use the LRT, written mathematically as

$$\Lambda = \frac{P(\tilde{\mathbf{Y}}|\mathbf{H}_1)}{P(\tilde{\mathbf{Y}}|\mathbf{H}_0)} \quad (25)$$

The probability density function (pdf) of the noise $n_i(r_\mu, m)$ is assumed Gaussian. The resolution cell in each radar output $g_i(x, R)$ is large compared to the center wavelength and for that reason the resolution cell contains many scatterers. Still in the sub-aperture beams $y_i(r_\mu, m)$ the resolution cell is large compared to the wavelength. With a high probability there are still many scatterers in the resolution cell of the sub-aperture beam. It is then appropriate to model the $q(r_\mu, m)$ pdf as Gaussian [34], as a consequence of the central limit theorem. The transformation from range to wave domain of a sequence is a summation, and a summation of Gaussian variables is a Gaussian variable. Therefore we use Gaussian pdfs for the clutter $\tilde{\mathbf{q}}$ and noise $\tilde{\mathbf{n}}$. Then under \mathbf{H}_0 :

$$P(\tilde{\mathbf{Y}}|\mathbf{H}_0) = \frac{1}{(2\pi)^{NM} |\tilde{\mathbf{C}}|} e^{-\tilde{\mathbf{Y}}^H \tilde{\mathbf{C}}^{-1} \tilde{\mathbf{Y}}} \quad (26)$$

and under \mathbf{H}_1 :

$$P(\tilde{\mathbf{Y}}|\mathbf{H}_1) = \frac{1}{(2\pi)^{NM} |\tilde{\mathbf{C}}|} e^{-\left(\tilde{\mathbf{Y}} - \tilde{\mathbf{A}}\right)^H \tilde{\mathbf{C}}^{-1} \left(\tilde{\mathbf{Y}} - \tilde{\mathbf{A}}\right)} \quad (27)$$

where $\tilde{\mathbf{C}}$ is the covariance matrix of $\tilde{\mathbf{Y}}$

$$\tilde{\mathbf{C}} = E\left[(\tilde{\mathbf{q}} + \tilde{\mathbf{n}})(\tilde{\mathbf{q}} + \tilde{\mathbf{n}})^H\right] \quad (28)$$

If we assume a moving point target we can simplify the measurement signal. The amplitude s_0 , and phase ϕ_0 , of a point target is independent of direction and frequency. The amplitude of the measured signal thus depends only upon range and is

approximately the sub-aperture center range, R_{cm} . The phase, ϕ_0 is random and distributed uniformly between 0 and 2π . Under the point target approximation the signal vector can be expressed as

$$\tilde{\mathbf{A}} = s_0 e^{j\phi_0} \tilde{\mathbf{A}} \quad (29)$$

Where $\tilde{\mathbf{A}}$ is the steering vector given by

$$\tilde{\mathbf{A}} = \begin{bmatrix} \frac{e^{-jk_0 r_1^i}}{R_{c1}^2} \\ \frac{e^{-jk_0(r_1^i + d(\cos \phi_1 - \cos \phi_1^i))}}{R_{c1}^2} \\ \vdots \\ \frac{e^{-jk_0(r_1^i + (L-1)d(\cos \phi_1 - \cos \phi_1^i))}}{R_{c1}^2} \\ \frac{e^{jk_0 r_1^i}}{R_{c1}^2} \\ \vdots \\ \frac{e^{-jk_{N-1}(r_1^i + d(\cos \phi_1 - \cos \phi_1^i))}}{R_{c1}^2} \\ \vdots \\ \frac{e^{jk_{N-1}(r_M^i + (L-1)d(\cos \phi_M - \cos \phi_1^i))}}{R_{cM}^2} \end{bmatrix} \quad (30)$$

Since ϕ_0 is random, the LRT is given by

$$E_\phi[\Lambda(\tilde{\mathbf{Y}})] = \int_0^{2\pi} \Lambda(\tilde{\mathbf{Y}}|\phi_0) \frac{d\phi_0}{2\pi} \quad (31)$$

According to [35] the test variable is

$$|\tilde{\mathbf{A}}^H \tilde{\mathbf{C}}^{-1} \tilde{\mathbf{Y}}|^2 \begin{cases} > \lambda & \text{decision for } \mathbf{H}_1 \\ < \lambda & \text{decision for } \mathbf{H}_0 \end{cases} \quad (32)$$

The clutter noise and the receiver noise can be considered as independent, giving

$$\tilde{\mathbf{C}} = E[\tilde{\mathbf{Y}}\tilde{\mathbf{Y}}^H] = E[\tilde{\mathbf{q}}\tilde{\mathbf{q}}^H] + E[\tilde{\mathbf{n}}\tilde{\mathbf{n}}^H] \quad (33)$$

The receiver noise samples $n_l(r_\mu, m)$ are independent both in local range r_μ and in between antenna channels l . The clutter signal $q_l(r_\mu, m)$ is dependent in l , but independent in m and r_μ . The sub-aperture beams are formed by non-overlapping samples which are independent, i.e. independent looks [34]. The wavenumber transformation will cause dependency on wavenumber k_n both for $\tilde{q}_l(k_n, \varphi_m)$ and $\tilde{n}_l(k_n, \varphi_m)$. However, if the number of radial samples N is sufficiently large then the dependency in k_n is weak [36], thus we assume the samples to be independent. The covariance will then simplify to

$$\tilde{\mathbf{C}} = \begin{bmatrix} \bar{\mathbf{C}}_{01} & 0 & \dots & 0 & 0 & \dots & 0 \\ 0 & \bar{\mathbf{C}}_{11} & \dots & 0 & 0 & \dots & 0 \\ \vdots & \vdots & \ddots & \vdots & \vdots & \dots & \vdots \\ 0 & 0 & & \bar{\mathbf{C}}_{(N-1)1} & 0 & \dots & 0 \\ 0 & 0 & \vdots & 0 & \bar{\mathbf{C}}_{12} & \dots & 0 \\ \vdots & \vdots & \vdots & \vdots & \vdots & \ddots & \vdots \\ 0 & 0 & 0 & 0 & 0 & \dots & \bar{\mathbf{C}}_{(N-1)M} \end{bmatrix} \quad (34)$$

where the diagonal matrixes $\bar{\mathbf{C}}_{nm}$ are given by

$$\bar{\mathbf{C}}_{nm} = E[\bar{\mathbf{q}}_{nm} \bar{\mathbf{q}}_{nm}^H] + E[\bar{\mathbf{n}}_{nm} \bar{\mathbf{n}}_{nm}^H] \quad (35)$$

and where the clutter $\bar{\mathbf{q}}_{nm}$ and the noise $\bar{\mathbf{n}}_{nm}$ are indexed in the same way as the measurement vector $\bar{\mathbf{Y}}_{nm}$, given by

$$\bar{\mathbf{Y}}_{nm} = \begin{bmatrix} \tilde{y}_1(k_n, \varphi_m) \\ \tilde{y}_2(k_n, \varphi_m) \\ \vdots \\ \tilde{y}_L(k_n, \varphi_m) \end{bmatrix} \quad (36)$$

The LRT is now reduced to

$$\left| \tilde{\mathbf{A}}^H \tilde{\mathbf{C}}^{-1} \tilde{\mathbf{Y}} \right|^2 = \left| \sum_{m=1}^M \sum_{n=0}^{N-1} \bar{\mathbf{A}}_{nm}^H \bar{\mathbf{C}}_{nm}^{-1} \bar{\mathbf{Y}}_{nm} \right|^2 = \begin{cases} > \lambda & \text{decision for } \mathbf{H}_1 \\ < \lambda & \text{decision for } \mathbf{H}_0 \end{cases} \quad (37)$$

and the steering vector simplifies to

$$\bar{\mathbf{A}}_{nm} = \frac{e^{-jk_n r'_m}}{R_{cm}^2} \begin{bmatrix} 1 \\ e^{-jk_n d(\cos \varphi_m - \cos \varphi'_m)} \\ \vdots \\ e^{-jk_n(L-1)d(\cos \varphi_m - \cos \varphi'_m)} \end{bmatrix} = \frac{e^{-jk_n r'_m}}{R_{cm}^2} \bar{\bar{\mathbf{A}}}_{nm}(\varphi'_m) \quad (38)$$

and the LRT can be written as

$$\left| \tilde{\mathbf{A}}^H \tilde{\mathbf{C}}^{-1} \tilde{\mathbf{Y}} \right|^2 = \left| \sum_{m=1}^M \frac{1}{R_{cm}^2} \sum_{n=0}^{N-1} e^{jk_n r'_m} \bar{\bar{\mathbf{A}}}_{nm}^H(\varphi'_m) \bar{\mathbf{C}}_{nm}^{-1} \bar{\mathbf{Y}}_{nm} \right|^2 = \left| \sum_{m=1}^M \frac{1}{R_{cm}^2} y_c(r'_m, m, \varphi'_m) \right|^2 = \begin{cases} > \lambda & \text{decision for } \mathbf{H}_1 \\ < \lambda & \text{decision for } \mathbf{H}_0 \end{cases} \quad (39)$$

using the notation

$$y_c(r, m, \varphi'_m) = \sum_{n=0}^{N-1} e^{jk_n r} \bar{\bar{\mathbf{A}}}_{nm}^H(\varphi'_m) \bar{\mathbf{C}}_{nm}^{-1} \bar{\mathbf{Y}}_{nm} \quad (40)$$

The vector $\bar{\mathbf{Y}}_{nm}$ includes the antenna channels at one wave domain point n and m . The product $\bar{\bar{\mathbf{A}}}_{nm}^H(\varphi'_m) \bar{\mathbf{C}}_{nm}^{-1} \bar{\mathbf{Y}}_{nm}$ will maximize the ratio between the target to clutter and noise [23]. Because clutter is correlated and often much stronger than the thermal noise we call it clutter suppression. The multiplication with $e^{jk_n r}$ and a summation in n is a transformation to time domain. In the following we call $y_c(r, m, \varphi'_m)$ the clutter suppressed sub-aperture beam. More details about Equation (40) are given in Appendix 1. In the LRT, the sum of $y_c(r'_m, m, \varphi'_m)$ in m is computed for the target location r'_m and the angle φ'_m to test if a moving target with speed v_t and heading α is present at minimum distance (x_0, ρ_0) .

In words the LRT in (25) is performed to test if a target is present at (x_0, ρ_0) with speed v_t and heading α . First the sub-aperture beams for all channels are formed at ground speed. There will be L sub-aperture beams, for each sub-aperture and each

sub-image. For the moving target there will be one clutter suppressed sub-aperture beam, $y_c(r'_m, m, \varphi'_m)$, at each sub-aperture m . The needed sub-aperture beams to compute $y_c(r'_m, m, \varphi'_m)$ and the target location r'_m are found considering relative speed, γ , according to section II.D. The next step is to combine the $y_c(r'_m, m, \varphi'_m)$ across m in (39). For each m the ratio between the target to clutter and noise will increase, and therefore the summation in m will increase the detectability.

Figure 8 demonstrates the moving target test. The clutter suppression stage computes the clutter suppressed sub-aperture beams $y_c(r'_m, m, \varphi'_m)$. These beams are combined over all available sub-apertures M , and is called the image formation, in Figure 8. The Figure also indicates the possibility to detect moving targets in $y_c(r'_m, m, \varphi'_m)$ using only one sub-aperture m , which will be used in the experimental data in section VI.

To test for other moving targets, the clutter suppressed sub-aperture beam has to be computed for each target and each m . Thus target detection is done through a filter bank referring to the target velocity vector, which can be justified mathematically by the likelihood test. However if the target appears in the same sub-aperture beam as other targets the covariance and the sub-aperture beams can be re-used, which saves computation.

In this paper we have assumed an ideal target that performs linear motion over the entire integration time and we can use all M clutter suppressed sub-aperture beams available. For real targets the approximation of linear motion is dependent on platform motion, target motion, and radar parameters. In many real situations the linear approximation is not valid over the long integration time associated with a WB system. However the number of used clutter suppressed sub-aperture beams in (39) is tunable and can be optimized to the situation. Therefore (39) can be used piecewise over the large aperture.

V. EXPERIMENTAL DATA

The method described in section III is developed for a WB SAR system. Because there are no multi-channel, wide-band data available, we, tested the algorithms on a narrow band data set. The narrow-band data set will give an insight into the wide-band method performance. The data used set comes from the C-band Andover radar system, developed by the SAR group in the Defence Evaluation Research Agency (DERA) in Malvern, United Kingdom.

The radar system operates at 5.7 GHz with a frequency bandwidth of 82 MHz and an antenna beamwidth of 8° . The system is able to digitally record fully coherent multiple phase center radar data with VV polarization and a PRF of 1.25kHz. The radar consists of two side-looking antennas displaced 0.49 meters in the along track direction. Both antennas are used as receivers and transmitters and the system alternates transmitting between the leading and trailing antennas. This gives the system a total of 4 channels: Channel A, Tx front Rx front; Channel B, Tx front Rx back; Channel C, Tx back Rx front and Channel D, Tx back Rx

back. The antenna phase center location will change between the channels. For Channel A the phase center will be at the leading antenna, for channel D the phase center will be at the trailing antenna; while channels B and C have a phase center approximately half way in between the front and back antenna. The clutter leakage caused by this approximation is negligible [33].

The data set used is from Porton Down in England and was collected in November 95. In this set there is one military vehicle moving along a tree lined track with a speed of 4-5 m/s in the across track direction and a unknown target with unknown speed and direction.

To illustrate the experimental data for one channel we form three small images by a frequency transform in slow time. These are shown in Figure 9. The images are formed over approximately 0.2 seconds at the slow time positions 500, 1750 and 3000, with a Fourier transform length of 256 samples. In all images the clutter has an offset in Doppler, which is caused by the narrow antenna beam pointing forward in the flight direction. The moving target is not separated from the clutter at 500, but at 1750 one of the moving targets is at the edge of the clutter signal, and at 3000 the two targets are well separated from the Doppler signal. The known military vehicle is at far range while an unknown vehicle is in near range. The different Doppler speeds of the moving target and the clutter cause the moving targets to separate from the clutter. We shall now test the proposed method to this data set.

VI. TARGET DETECTION IN DERA DATA

DERA provided four channel pulse compressed radar data for this analyses. From these, ground speed processed sub-aperture beams were formed for each antenna channel. The antenna center, not the ground, were chosen as reference point due to the lack of high quality positioning data. The sub-aperture length and sub-image size was selected in order to satisfy the far field approximation. The geometry of the sub-aperture and the sub-beams are given in Figure 10.

For target detection we used the method described in section IV. In real data we do not know the target position (x_0, ρ_0) , speed v_t and heading α . Therefore we have to test many different possibilities in these parameters. In this data set with no high quality positioning data we have chosen to test without the summation of sub-apertures m i.e. $M=1$. To test if a target is present in direction φ' at sub-aperture angle φ we form a sub-aperture beam $y_c(r, 1, \varphi')$. By a fft of $\bar{\mathbf{A}}_n^H(\varphi')\bar{\mathbf{C}}_n^{-1}\bar{\mathbf{Y}}_n$ in n we are able to test if there is a target present for all possible r .

The proposed method uses the sub-aperture beams in the frequency domain and the statistics of the noise and the clutter signal. To estimate the statistics we divided the range samples in the sub-aperture beams into eight range bins, according to

Figure 10. These bins were transformed to the frequency domain. Under the assumption that the clutter signal is much stronger than the target signal, the covariance was estimated between the channels by the maximum likelihood estimate of the covariance

$$\bar{\mathbf{C}}_n^p = E\left[\bar{\mathbf{Y}}_n^p \bar{\mathbf{Y}}_n^{pH}\right] \approx \frac{1}{8} \sum_{p=1}^8 \bar{\mathbf{Y}}_n^p \bar{\mathbf{Y}}_n^{pH} \quad (41)$$

where p is the index of the sub-aperture bin. The algorithm will automatically compensate for the differences between the antenna channels. Combined with equation (41), we used CFAR normalization to ensure a constant false alarm.

VII. RESULTS

To detect the moving targets in the data set we used the method described in section IV. The selected region of slow time samples was between 0-4000 in the data set. This is an extended data set compared to that shown in images in Figure 9. Especially, in samples 0-500 the targets are surrounded by stronger clutter than shown in the images in that Figure. The sub-aperture beams were formed using equation (5) under far field approximation. The sub-image size was selected to 10 meters in azimuth at the range distance of 2100 meters, which corresponds to an angle of approximately 0.27° between the beams. In Figure 11 the sub-aperture beam for one antenna channel, at 250 with angle 88.08° , is shown. The sub-aperture contains a moving target. However, it is not possible to detect the moving targets due to the strong clutter.

The sub-aperture beams for all channels were calculated. From these beams the covariance was estimated according to (41). The clutter suppressed sub-aperture beam was calculated using the covariance, the steering vector and the computed sub-aperture beams. The clutter suppressed sub-aperture beam shown in Figure 12 is over the same area as the sub-aperture beam in Figure 11. The moving target, not detectable in Figure 11, appears clearly in the beam, and can be detected. The steering vector was selected to optimize the signal to clutter noise ratio (SCNR). The results of target detection from different sub-aperture beams are shown in Figures 13 and 14 as a function of Doppler angle φ (Figure 6). The unknown near-range moving target is given in Figure 13 and the military target is given in Figure 14. The figures give the Clutter to Noise Ratio (CNR), the SCNR for one sub-aperture beam (SCNR_{nf}), and the SCNR for the clutter suppressed sub-aperture beam (SCNR_f). The CNR is found by the ratio between the clutter estimate and the noise estimate beam in Figure 10. The method to estimate SCNR_f and SCNR_{nf} is given in the appendix 2. When the SCNR is small the estimate will have large uncertainty and we have used standard deviation as the confidence interval of the estimates. The derivation of the std of SCNR is provided in the appendix 2. Because of the strong

clutter at low Doppler angles the $SCNR_{nf}$ is very small, and the standard deviation is so large that the lower confidence limit goes to negative infinity. Therefore in Figure 14, seven $SCNR_{nf}$ low angle measurements are averaged to one point. The average is 0.37 dB and the uncertainty of the average below 0dB is now only 4dB.

As seen in Figures 13 and 14, the CNR decreases as the angle φ increases over the measured interval. The $SCNR_f$ is nearly stable while the $SCNR_{nf}$ increases with angle. The clutter suppression is estimated from the Figures 13 and 14 by the ratio of $SCNR_f$ and $SCNR_{nf}$ [37]. We then use a real moving target to estimate the clutter suppression. The approach will underestimate the clutter suppression due to the fact that the $SCNR_f$ depends on target parameters, such as speed and vibrations, and radar system parameters such as system stability. If the target has a slow speed the clutter suppression algorithm will also suppress the target.

Other authors have implemented a synthetic moving target in their SAR data to measure the clutter suppression [38,39]. The synthetic target will be an ideal target that has a stability in scattering and motion that no real targets can achieve. The synthetic target will not be influenced by imperfections in the radar system. With a synthetic target we would therefore overestimate the clutter suppression. For this article, we have chosen a real target which give a proper estimate when the backscattering is strong and the target speed sufficiently high. For a $SCNR_{nf}$ around 0dB the lower confidence limit goes towards minus infinity, which implies the $SCNR_{nf}$ is likely to be overestimated. An underestimation of $SCNR_f$ and an overestimation of $SCNR_{nf}$ means an underestimation of the clutter suppression.

The clutter suppression from Figures 13 and 14 was found to be greater than 20dB, and for some sub-apertures the suppression was 25dB. These results are a slightly lower than the 23-30dB reported by [32,38,40]. However these papers do not describe the clutter estimate procedures, confidence or statistical background used making comparison of these techniques difficult. For example, reference [38] uses synthetic moving targets as opposed to our experiments as use real targets. Real targets give an under estimation of clutter suppression. In addition performance is dependent on the test site. Note that clutter suppression is bound by the CNR, which in Figure 13 and 14 is just over 20 dB.

VIII. DISCUSSION

To detect a moving target in a WB SAR system we combine multi-antenna channel fast backprojection SAR processing with moving target detection, by a space-time approach. There are many fast backprojection methods, such as the ones given in Section II.A; LBP, FBPA, QBP and FFBP. The aim of this work is to perform GMTI using the multi stage algorithm FFBP. However, the derivation of our technique using LBP is more mathematically straight forward. Therefore we use LBP in our derivation. The results given here are also valid for FFBP.

The developed method gives the possibility to detect moving targets, suppress the clutter signal, and to form images of the moving target. In the algorithm we assume the target has linear motion during illumination. The quality of this approximation is dependent on platform motion, target motion, distance to target and radar parameters such as frequency. It is probably invalid for many targets in a WB SAR system, since the more time spent illuminating the target increases the chance of non-linear motion. However we can select a shorter integration time where the linear approximation is valid and we are free to choose the number of sub-apertures, M , used in the test (39). In particular the variable M fits very well with the multi-stage backprojection algorithms such as FFBP. In the future further work is needed to increase the integration time and the number of clutter suppressed sub-aperture beams in the test.

In the experimental data set clutter suppression was found to be approximately equal to the limit by the CNR of approximately 20dB. The image formation phase of the clutter suppressed sub-aperture beams were not implemented on the experimental data. In the data set the sub-apertures have a length of approximately 10 meters, corresponding to approximately 0.1 seconds in time. In the used C-band system, a moving target will most likely have near linear motion with respect to the platform for more than 0.1 seconds thus we assume 1 second and chose $M=10$. This will increase $SCNR_f$ and this increase is dependent on relative speed. The integration time under linear motion assumption is dependent on radar frequency and motion of the target and platform.

IX. CONCLUSION

In this article we have presented a method for detecting moving targets in a WB SAR system with an antenna array. WB implies both an ultra wide frequency band and wide antenna beam. In WB SAR systems, time domain backprojection has shown to be very effective. The developed method combines fast backprojection SAR processing methods with moving target detection. In fast backprojection methods the SAR image formation process is divided into two steps, beam forming and image formation.

The LRT is found from the sub-aperture beams from the L channels of the antenna array. The proposed test performs clutter suppression in the sub-aperture beams by space-time processing and combines the clutter suppressed sub-aperture beams to form a test image. The combination of clutter suppressed sub-aperture beams is the same as performing SAR image formation of a moving target, which requires the relative speed of the target.

The proposed target detection method forms sub-aperture beams at ground speed, performs clutter suppression, and finally combines the clutter suppressed sub-aperture beams by relative speed. This means that many different targets with different locations and speeds can be testing using the same covariance matrix and sub-aperture beams. This reuse of computed beams saves computational resources [2].

The proposed method assumes linear motion of the moving target over the long integration time needed in a WB SAR system. How good this approximation is depends upon the target and radar motion as well as the radar parameters such as frequency. For many situations the approximation is not good when the illuminating time for the target increases, because of the increase in chance for non-linear motion. However, in the developed method it is possible to select pieces of the long aperture where the linear approximation can be used. To increase the resolution of the moving target, further work has to be done to increase the integration time by non-linear motion considerations.

The proposed target detection method was developed for WB SAR systems. Unfortunately, there are no multi-channel WB data available. Therefore the method was tested using narrow band data. The image formation, i.e. the combination of clutter suppressed sub-aperture beams by relative speed, was not implemented in this data set. The results of the clutter suppressed sub-aperture beams indicate that clutter suppression is approximately 20-25 dB and equal to the clutter to noise ratio, as expected.

X. APPENDIX 1

In Equation (14) the sub-aperture beam for antenna channel l is given. In this paper we use the sampled sub-aperture beam given in vector form by

$$\mathbf{y}_l(m) = \begin{bmatrix} y_l(r_0, m) \\ y_l(r_1, m) \\ \vdots \\ y_l(r_{N-1}, m) \end{bmatrix} \quad (42)$$

where r_μ is the sample points in local range given by $r_\mu = r_0 + \Delta r_s \mu$, and r_0 is a constant offset, Δr_s is the sampling interval, and μ is the sampling index from 0 to $N-1$. By the discrete wave transformation the wave transformed sub-aperture beam is given by

$$\tilde{y}_l(k_n, m) = \frac{1}{N} \sum_{\mu=0}^{N-1} e^{-jk_\mu r_\mu} y_l(r_\mu, m) \quad , n=0, 1, \dots, N-1 \quad (43)$$

where k_n is wave domain points given by $k_n = k_0 + \Delta k_s n$, and k_0 is the lowest used wave number and $\Delta k_s = 2\pi/N\Delta r_s$. The inverse transformation is then

$$y_l(r_\mu, m) = \sum_{n=0}^{N-1} e^{jk_n r_\mu} \tilde{y}_l(k_n, m) \quad , \mu=0, 1, \dots, N-1 \quad (44)$$

The wave transformed sub-aperture beam in vector form $\tilde{\mathbf{y}}_l(m)$ is given by

$$\tilde{\mathbf{y}}_l(m) = \begin{bmatrix} \tilde{y}_l(k_0, m) \\ \tilde{y}_l(k_1, m) \\ \vdots \\ \tilde{y}_l(k_{N-1}, m) \end{bmatrix} \quad (45)$$

In the Equation (40) we have the product

$$\bar{\mathbf{A}}_{nm}^H(\varphi'_m) \bar{\mathbf{C}}_{nm}^{-1} \bar{\mathbf{Y}}_{nm} \quad (46)$$

where $\bar{\mathbf{A}}_{nm}(\varphi'_m)$ is the steering vector given in Equation (38), $\bar{\mathbf{C}}_{nm}$ is the covariance given in Equation (35) and $\bar{\mathbf{Y}}_{nm}$ is the measurement vector for one point in wave domain formed of the L antenna channels given in Equation (36). At every n and m the product $\bar{\mathbf{A}}_{nm}^H(\varphi'_m) \bar{\mathbf{C}}_{nm}^{-1} \bar{\mathbf{Y}}_{nm}$ will maximize the signal to clutter noise ratio (SCNR) [23]. The product will maximize the signal described by the steering vector compared to the clutter and noise described by the covariance. In words we combine the antenna channels in $\bar{\mathbf{Y}}_{nm}$ such that we get the best possible SCNR for the target described by $\bar{\mathbf{A}}_{nm}(\varphi'_m)$. We can then form a sub-aperture beam with wave components

$$\tilde{y}_c(k_n, m, \varphi'_m) = \bar{\mathbf{A}}_{nm}^H(\varphi'_m) \bar{\mathbf{C}}_{nm}^{-1} \bar{\mathbf{Y}}_{nm} \quad (47)$$

and all n components in the sub-aperture m has maximized SCNR given by

$$\tilde{\mathbf{y}}_c(m) = \begin{bmatrix} \tilde{y}_c(k_0, m, \varphi'_m) \\ \tilde{y}_c(k_1, m, \varphi'_m) \\ \vdots \\ \tilde{y}_c(k_{N-1}, m, \varphi'_m) \end{bmatrix} \quad (48)$$

in vector form. For a particular r in (40) we have

$$\sum_{n=0}^{N-1} e^{jk_n r} \tilde{y}_c(k_n, m, \varphi'_m) \quad (50)$$

Comparing the inverse transformation in (46) this is just a transformation from wave domain to range domain.

$$y_c(r, m, \varphi'_m) = \sum_{n=0}^{N-1} e^{jk_n r} \tilde{y}_c(k_n, m, \varphi'_m) \quad (51)$$

The range domain sub-aperture beam will also have maximum SCNR and we therefore call it the clutter suppressed sub-aperture beam.

XI. APPENDIX 2

To analyze the performance of the GMTI method used in this paper we need to estimate SCNR_{nf} , SCNR_f and CNR. This appendix describes how these estimates and their accuracy are determined.

The SCNR_f was determined from the clutter suppressed sub-aperture beam using the following procedure. The peak energy from the target was determined in the clutter suppressed sub-aperture beam. The clutter and noise energy $\bar{\sigma}_{\text{CN}-f}$ was found by averaging all samples, excluding the samples of the target and its surroundings. The target energy is estimated from the peak energy after subtracting $\bar{\sigma}_{\text{CN}-f}$. The SCNR_f was determined from the ratio between the target energy and $\bar{\sigma}_{\text{CN}-f}$.

The SCNR_{nf} is found in a sub-aperture beam connected to one antenna channel. The SCNR_{nf} is more complicated to estimate than SCNR_f , due to the strong clutter surrounding the target. To find the peak value of the moving target in the sub-aperture beam we used the target location found in the clutter suppressed sub-aperture beam. The range gate of the moving target in the clutter suppressed sub-aperture beam gives the range gate in the sub-aperture beam, and from this the peak energy was found. The clutter and noise energy in the sub-aperture beam, $\bar{\sigma}_{\text{CN}-\text{nf}}$, was found in the same way as in the clutter suppressed sub-aperture beam. Finally the SCNR_{nf} was computed in the same way as for SCNR_f using the peak energy and $\bar{\sigma}_{\text{CN}-\text{nf}}$.

The estimate of CNR is determined from $\bar{\sigma}_{\text{CN}-\text{nf}}$ and the thermal noise, which is estimated from a sub-aperture beam far from the main antenna footprint, as seen in Figure 10.

The estimate of SCNR_f has high accuracy due to the large ratio (>20dB). However, the estimate of SCNR_{nf} is more complicated because of the strong clutter backscattering. The unknown phase relation between target and clutter will cause a

large uncertainty in the estimate. Assuming the peak method [41], the relative mean squared error of the SCNR estimate is given by

$$\varepsilon^2 = \frac{1 + \frac{1}{N_s}}{SCNR^2} + \frac{2}{SCNR} \quad (52)$$

where N_s is the number of independent clutter samples. From the relative mean squared error we get the variance and the mean. To indicate the accuracy in the estimate of SCNR a top and a bottom limit is given by the variance. The variance is estimated by using equation (52). When the SCNR goes below 4 dB, the relative mean squared error increases over 1. In Figure 14 we have therefore used all independent samples of $SCNR_{nr}$ between 87.8 to 89.6 degrees to estimate the mean and variance given in one point.

XII. ACKNOWLEDGEMENT

We would like to acknowledge, Defence Evaluation Research Agency (DERA) in United Kingdom (UK) and the UK MoD Coporate Research Programme for the C-band data. Especially the Author would like to thank Dr. Mark Williams and Darren Coe both at DERA for their help and assistance with this data set. We also acknowledge Dave Murray at NASoftware UK for processing at DERA.

The author is grateful to Adj. Prof. Lars Ulander, Swedish Defence Research Institute (FOI) and Prof. Mats Viberg at Chalmers University of Technology for ideas and useful comments on this paper. The Author is also grateful to Ph.D. Bill Pierson U.S. Air Force Research Laboratory (AFRL) for the help with the English language in the article and to Gunnar Stenström at FOI for the transformation of the DERA data to a readable data format.

XIII. REFERENCES

- [1] M. Soumekh, "Moving Target Detection in Foliage Using Along Track Monopulse Synthetic Aperture Radar Imaging", IEEE Transactions on Image Processing, Vol. 6, pp. 1148-1162, 1997
- [2] M.I. Pettersson, "Focusing of Moving Targets in an Ultra-wide band SAR GMTI System", Proc. of EUSAR 2000, 3rd European Conference on Synthetic Aperture Radar, Germany, 2000, pp. 837-840

- [3] J.A. Fawcett, "Inversion of N-dimensional spherical averages", SIAM J. of Appl. Math., Vol. 45, No. 2, 1985, pp 336-341
- [4] L.E. Andersson, "On Determination of a Function from Spherical Averages", SIAM J. of Appl. Math., Vol. 19, No. 1, 1988, pp 214-341
- [5] H. Hellsten, L.M.H. Ulander, A. Gustavsson and B. Larsson, "Development of VHF CARABAS II SAR", SPIE Conference on Radar Sensor Technology, SPIE vol. 2747, Orlando, FL, USA 8-9 April, 1996, pp. 48-60
- [6] H. Hellsten and L.M.H. Ulander, "Airborne Array Aperture UWB UHF-Motivation and System Consideration", Proceedings of the 1999 IEEE Radar Conference –Radar to the next millenium, Waltham, 1999, pp. 47-53
- [7] L.M.H. Ulander and H. Hellsten, "Low-frequency Ultra wideband Array-Antenna SAR for Stationary and Moving Target Imaging", Proc. SPIE Conference on Radar Sensor Technology IV, Vol. 3704, Orlando, Florida;1999, pp. 149-157
- [8] L.M.H. Ulander, P.O. Frörlind, A. Gustavsson, H. Hellsten, and B. Larsson, "Detection of Concealed Ground Targets in CARABAS SAR Images using Change Detection", Proceedings of SPIE Conference on Algorithms for Aperture Radar Imagery VI, 3721, Orlando, 1999, pp. 243-252
- [9] L.M.H. Ulander, "Approaching the Wavelength Resolution Limit in Ultra-wideband VHF-SAR", Proc. of the PIERS Workshop on Advances in Radar Methods, 1998, Baveno, Italy, pp. 83-85
- [10] L.M.H. Ulander and H. Hellsten, "A New Formula for SAR Spatial Resolution", AEÜ Int. J. Electron. Commun., Vol. 50, No. 2, 1996, pp. 117-121
- [11] L.M.H. Ulander and P.-O., Frörlind, "Precision Processing of CARABAS HF/VHF-band SAR Data", Proc. of IGARSS'99, Vol. 1, 1999, Hamburg, Germany, pp.47-49
- [12] O. Seger, M. Herberthson and H. Hellsten: "Real Time SAR Processing of Low Frequency Ultra Wide Band Radar Data", Proc. EUSAR'98, Friedrichshafen, 1998, pp. 489-492.
- [13] A.F. Yegulalp, "Fast backprojection Algorithm for Synthetic Aperture Radar", Proc. of 1999 IEEE Radar Conference, Waltham, Massachusetts, 1999, pp. 60-65
- [14] J. McCorkle and M. Rofheart, "An order $N^2 \log(N)$ backprojector algorithm for focusing wide-angle wide-bandwidth arbitrary-motion synthetic aperture radar", Proc. of SPIE Conference on Radar Sensor Technology, Vol. 2747, Orlando, 1996, pp. 25-36
- [15] Nilsson S., "Application of fast backprojection techniques for some inverse problems of integral geometry", Linköping studies in Science and Technology. Dissertation No. 499, Department of Mathematics, Linköping University, Linköping, Sweden, ISBN 91-7219-021-3, 1997

- [16] L.M.H. Ulander, H. Hellsten and G. Stenström, "Synthetic-Aperture Radar Processing using Fast Factorised Back-Projection", IEEE Transactions on Aerospace and Electronic Systems, Vol. 39, No. 3, July 2003, pp.760-776
- [17] B.C. Barber, "Theory of digital imaging from orbital synthetic-aperture radar", International Journal of Remote Sensing, Vol. 6, 1985, pp 1009-1057
- [18] M.I. Pettersson, L.M.H. Ulander and H. Hellsten, "Simulations of ground moving target indication in a ultra-wideband and wide-beam SAR system", Proc. SPIE Conference on Radar Processing., Technology and Application IV, Vol. 3810, Denver, 1999, pp. 84-95
- [19] R. K. Raney: "Synthetic Aperture Imaging Radar and Moving Targets", IEEE Trans. Aerospace and Electronic Systems, Vol. AES-7, No. 3, 1971, pp. 499-505
- [20] M.I. Pettersson and L.M.H. Ulander, "Jammer suppression in an ultra-wideband and widebeam SAR system", 5th International Conference on Radar systems, Radar'99, 1999, Brest, France
- [21] Merrill. I. Skolnik, *Radar Handbook*, New-York: McGraw-Hill, 1970
- [22] B. Widrow, P.E. Mantey, L.J. Griffiths and B.B. Goode, "Adaptive Antenna Systems", Proceedings of IEEE, Vol. 55, No. 12, 1967, pp. 2143-2159
- [23] L.E. Brennan, J.D. Mallett and, I.S. Reed, "Adaptive Arrays for airborne MTI Radar", IEEE Transactions on Antennas and Propagation, Vol. 24, No. 5, 1976
- [24] J. Ward, "Space -Time Processing for for Airborne Radar", Lincoln lab, Massachusetts institute of technology, Technical Report No. 1015, 1994
- [25] R. Klemm, *Space- Time Adaptive Processing; principles and applications*, London: The Institution of Electrical Engineers, 1998
- [26] J.H.G. Ender, "Space-time processing for multichannel synthetic aperture radar", IEE Electronics & communication engineering journal, 1999, pp. 29-38
- [27] S. Barbarossa, "Detection and imaging of moving objects with synthetic aperture, Part 1: Optimum detection and parameter estimation theory", IEE Proceedings-F, Vol. 139, No. 1, 1992, pp 79-88
- [28] S. Barbarossa, and A. Farina, "Detection and imaging of moving objects with synthetic aperture, Part 2: Joint time-frequency analysis by Wigner-Ville distribution", IEE Proceedings-F, Vol. 139, No. 1, 1992, pp. 89-97
- [29] E. D'Addio, M. Di Bisceglie, and S. Bottalico, " Detection of moving objects with airborne SAR", Signal Processing, Vol. 36, 1994, pp. 149-162
- [30] J.H.G. Ender, "Detectability of slowly moving targets using a multi-channel SAR with an along-track antenna array", SEE/IEE Collegium on SAR-93, 1993, pp. 18-22

- [31] J.H.G. Ender, "Experimental Results achieved with the Airborne Multi-Channel SAR System AER-II", EUSAR'98, European conference on Synthetic Aperture Radar, Friedrichshafen, 1998, pp. 315-318
- [32] Darren J. Coe and Richard G. White, "Experimental Moving target Detection Results from a Three-Beam Airborne SAR", *AEÜ Int. J. Electron. Commun.*, Vol. 50, No. 2, 1996, pp. 157-164
- [33] M.I. Pettersson: "Extraction of moving ground targets by a bistatic ultra-wideband and -widebeam SAR system", *IEE Proc. Radar, Sonar and Navigation*, Vol. 148, No. 1, 2001, pp. 35-40
- [34] C. Oliver and S. Quegan, *Understanding Synthetic Aperture Radar Images*, London: Artech House, 1998
- [35] W.S. Chen and I.S. Reed, "A New CFAR Detection Test for Radar", *Digital Signal Processing*, Vol. 1, No. 4, pp. 198-214, 1991
- [36] L. Ljung, *System Identification, Theory for the user*, Upper Saddle River: Prentice Hall PTR, 1999
- [37] F.E. Nathanson, *Radar design principles- Signal processing and the Environment*, New York: McGraw-Hill book company, 1969
- [38] A. Farina, L. Timmoneri, R. Graziana, F. Lee, "Adaptive space-time processing with systolic algorithm: Experimental Results using recorded live data", *Proceedings Radar 95, IEEE International Radar conference, Virginia, USA, 1995*, pp. 495-602.
- [39] A. Farina, P. Lombardo and M. Pirri, "Nonlinear STAP processing", *IEE Electronics & communication engineering journal*, 1999, pp. 41-48
- [40] E.F. Stockburger and D.N. Held, "Interferometric moving ground target imaging" *Proceedings Radar 95, IEEE International Radar conference, Virginia, USA, 1995*, pp. 495-602.
- [41] L.M.H. Ulander: "Accuracy of using Point Targets for SAR Calibration", *IEEE Transactions on Aerospace and Electronic Systems*, Vol. 27, No. 1, 1991

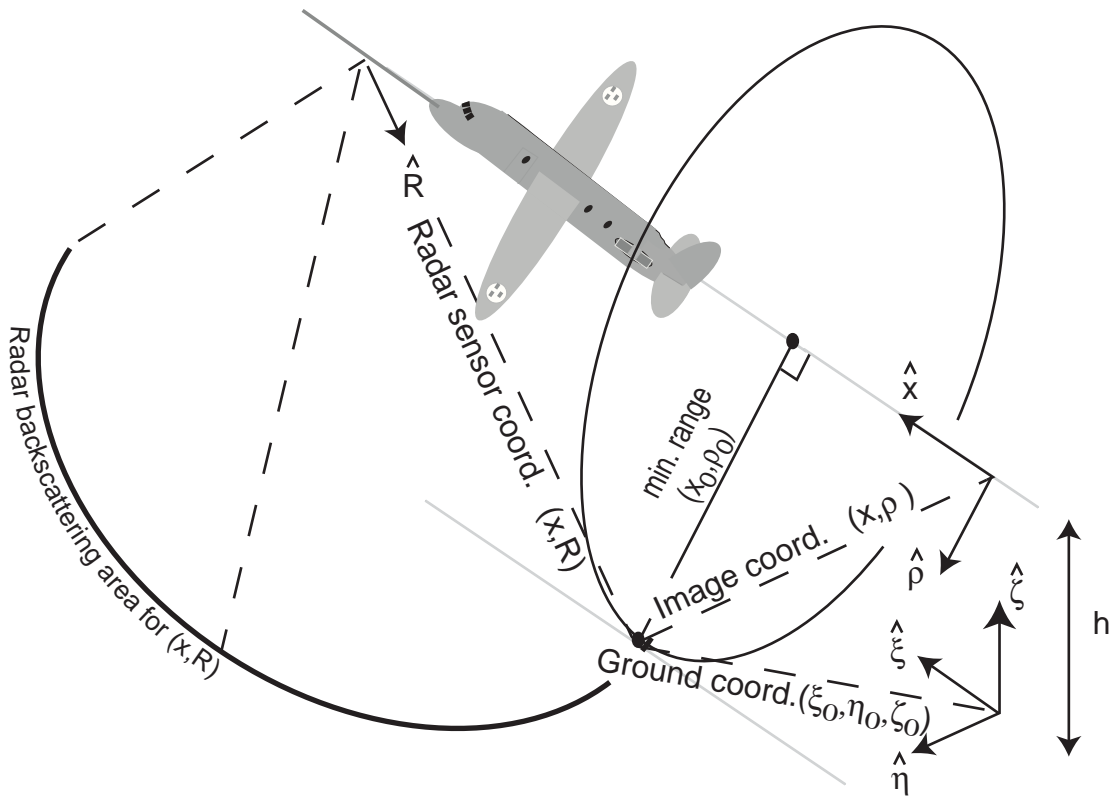


Figure 1. The three used coordinate systems, the ground coordinate system (ξ, η, ζ) , the radar coordinate system (x, R) with x cross range and R range, and the image coordinate system for a stationary target (x, ρ) .

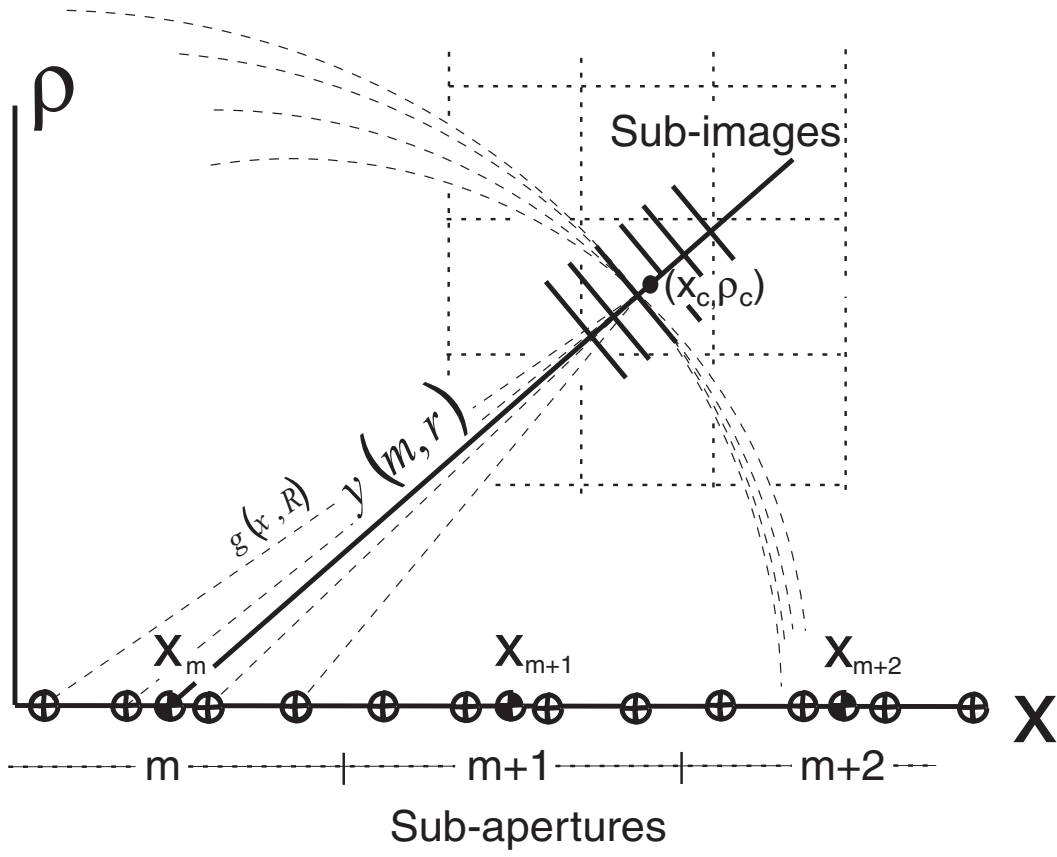


Figure 2. The sub-images and the sub-apertures in LBP. The radar output $g(x, R)$ is sampled at \oplus . From the radar samples, sub-aperture beams are calculated at every \odot (sub-aperture center position x_m) over each sub image. At x_m the sub-aperture beam $y(m, r)$ is formed over the sub image with center coordinate (x_c, ρ_c) .

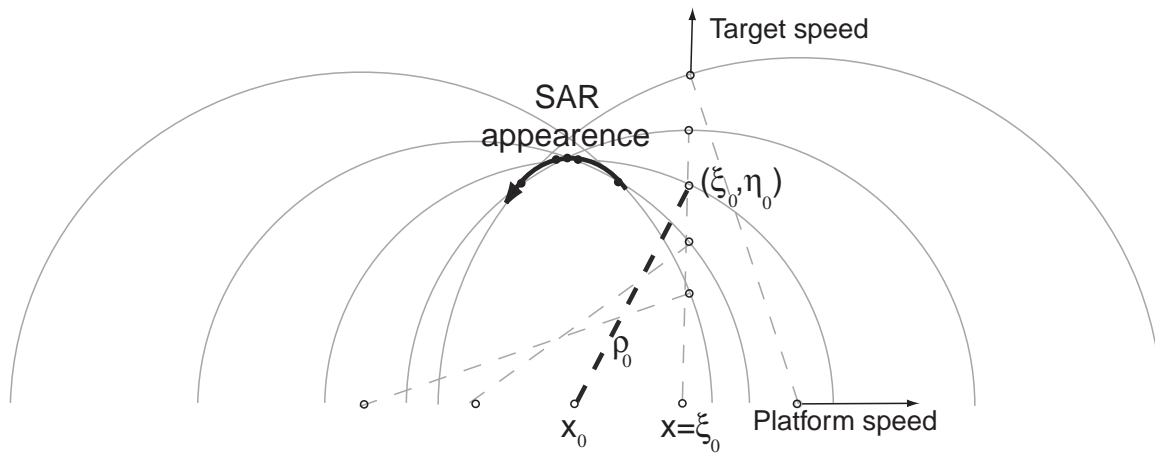


Figure 3. The displacement and defocusing of a moving target in a SAR image processed for stationary targets [30]. At each radar position x there will be a location of the moving target (ξ, η) . The target and the platform location at five points are shown and their connected distance. At one particular point x_0 the minimum distance ρ_0 occur. The figure is a geometrical illustration that the moving target will be unfocused and displaced at point (x_0, ρ_0) .

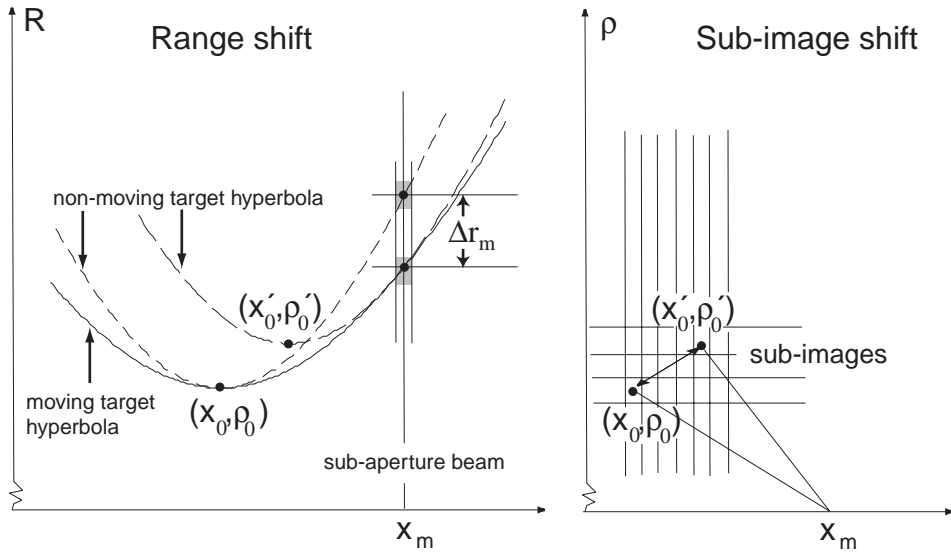


Figure 4. Focusing with relative speed γ using sub-beams calculated for ground speed. The location of the moving target at (x_0, ρ_0) in sub-aperture x_m can be found from the position (x'_0, ρ'_0) . If the moving target speed is large there will be a sub-image shift during long integration.

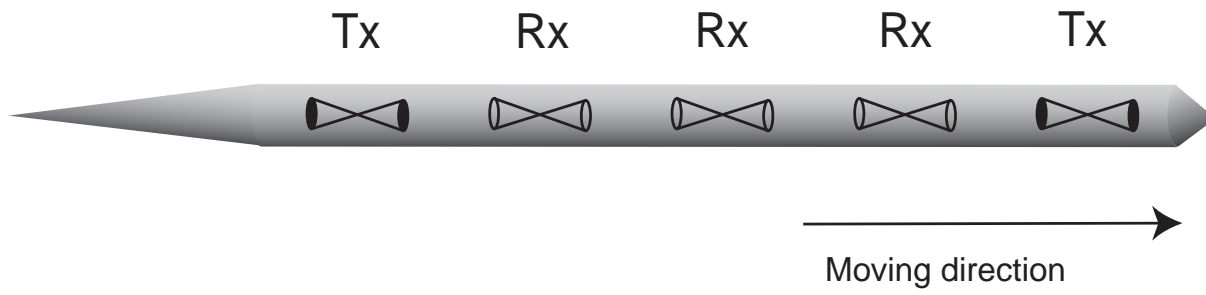


Figure 5. The LORA antenna with two transmitting channels (Tx) and three receiving channels (Rx).

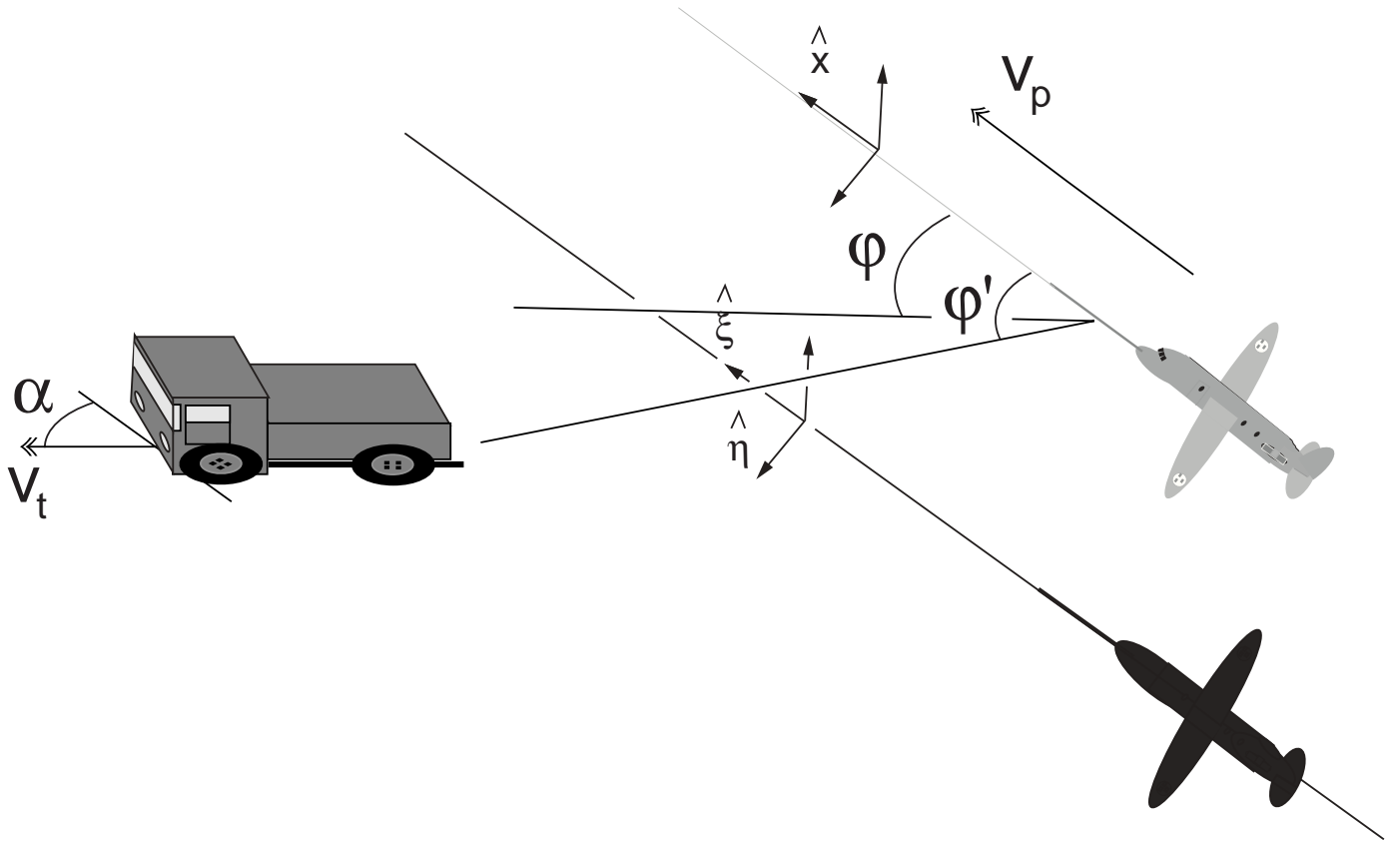


Figure 6. The moving target heading and speed in the ground coordinate system $(v_x, v_y, 0) = v_t (\cos \alpha, \sin \alpha, 0)$. The direction from the plane to the moving target is φ' . The sub-aperture beams are formed according to Doppler and the moving target will appear in a sub-aperture at direction φ .

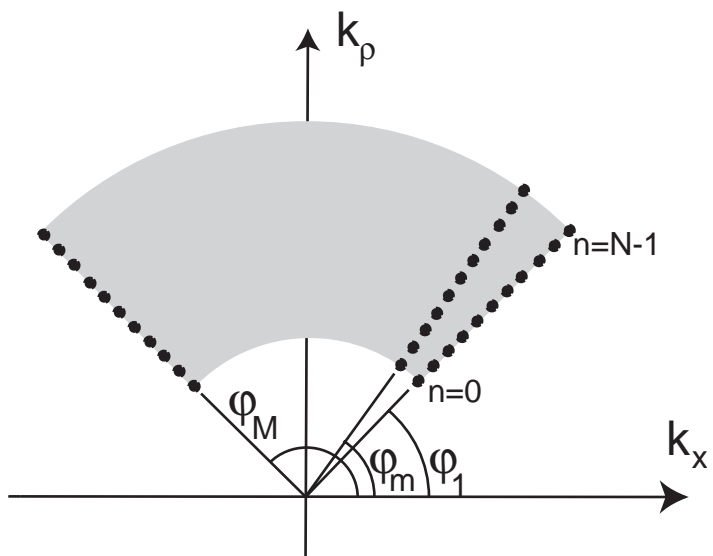


Figure 7. The wavenumber space. The sub-aperture beams are located in the image wavenumber space.

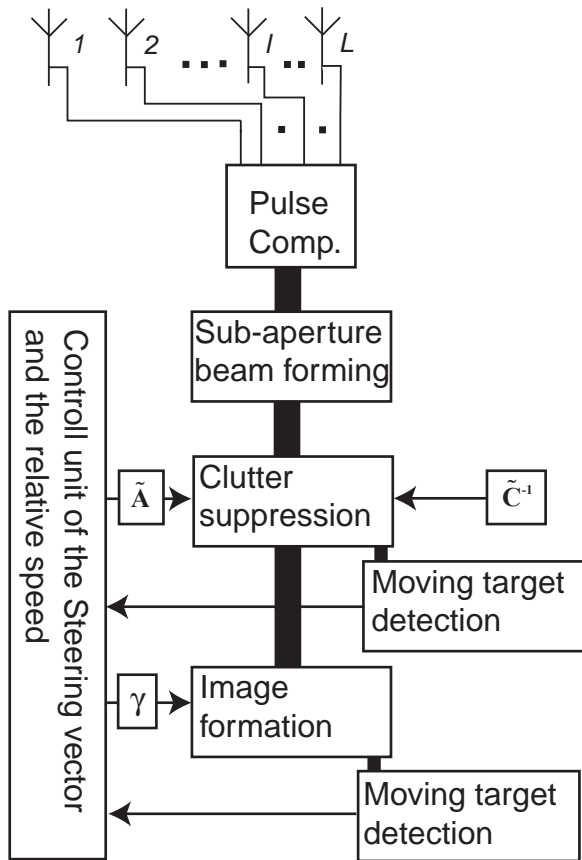


Figure 8. The moving target detection scheme. After pulse compression, sub-aperture beams are formed at ground speed for each antenna channel (section II.B and section III). Clutter suppressed sub-aperture beams are formed by the L sub-aperture beams by covariance and the target steering vector (section IV.B). The clutter suppressed sub-aperture beams are combined during image formation considering relative speed (section II.D). A moving target can be detected using only one clutter suppressed sub-aperture beam and to increase the detectability the beams are combined in image formation (section IV).

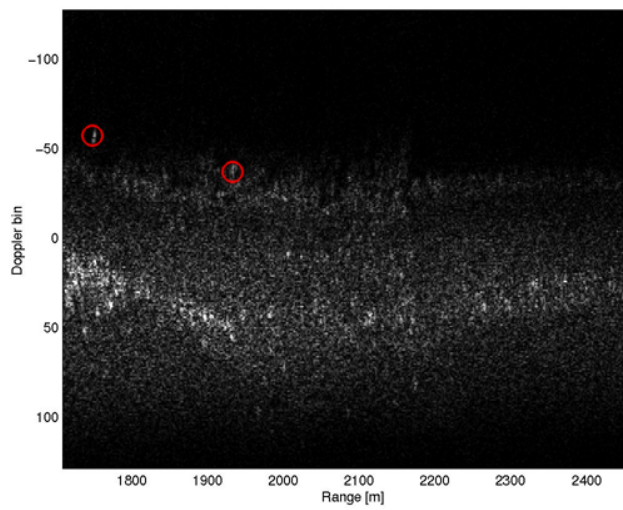
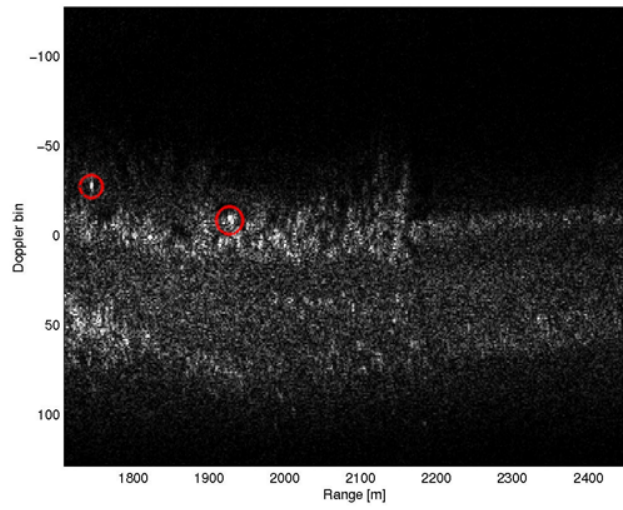
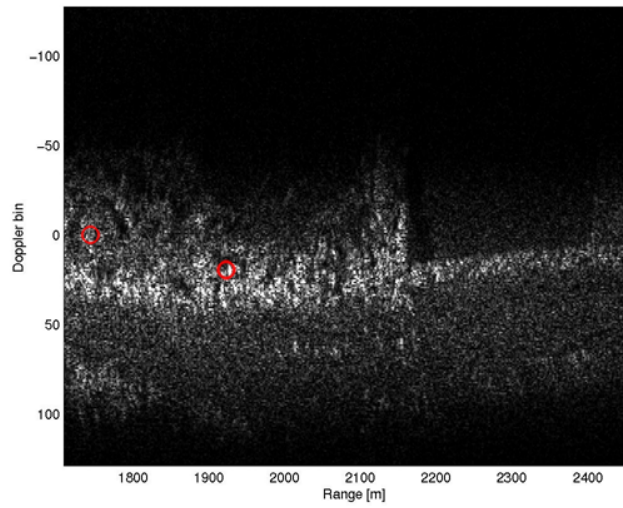


Figure 9. Doppler-range images. The two moving targets appear clearly when they are well separated in Doppler from the clutter.

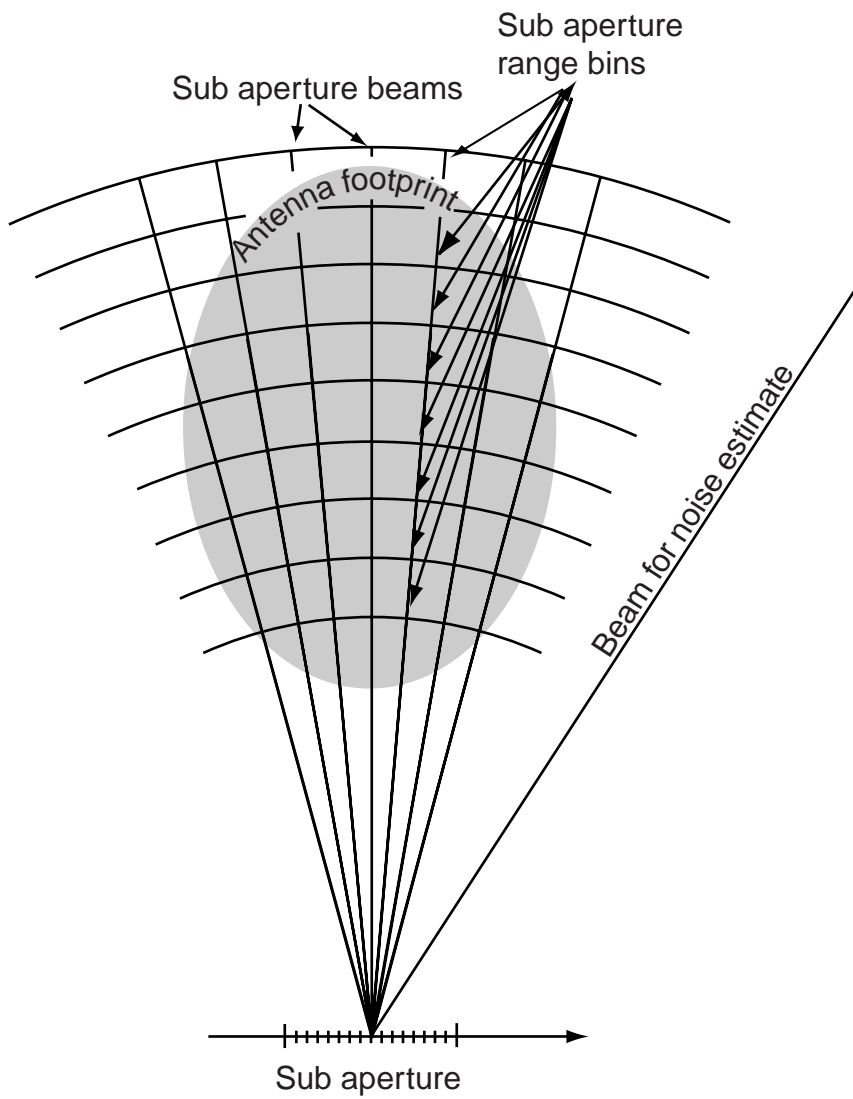


Figure 10. Sub-aperture beams connected to one sub-aperture and the antenna footprint. Each sub-aperture beam for each channel over the antenna footprint were divided into range bins used to estimate the covariance matrix. One sub-aperture beam was formed over the smallest antenna gain for the noise estimate to the clutter to noise ratio (CNR).

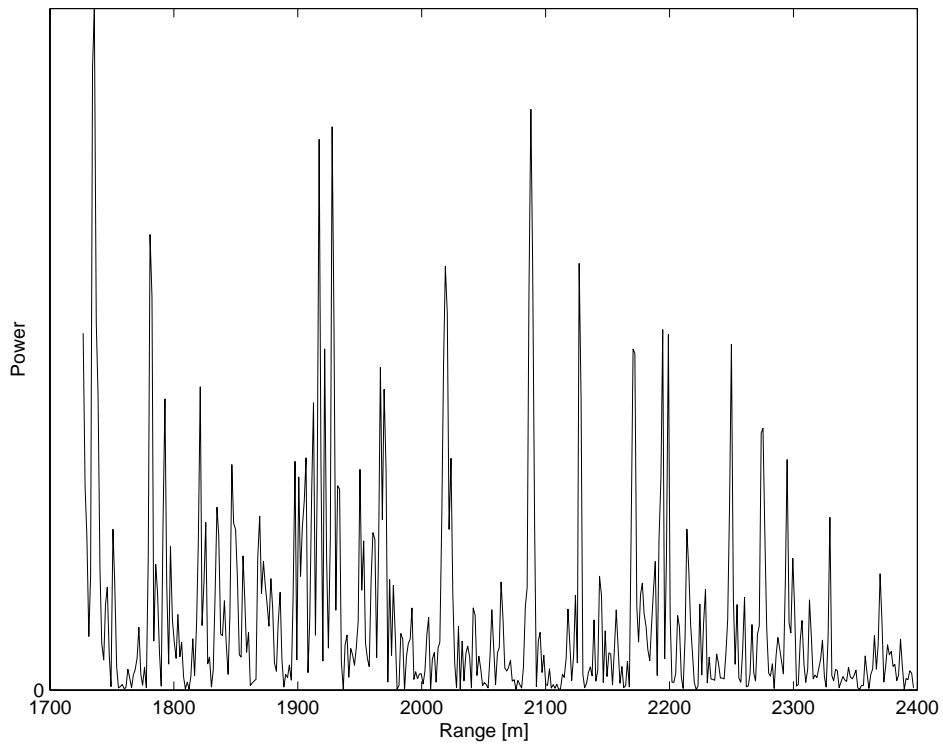


Figure 11. Sub-aperture beam formed at sample 250 with angle 88.08° for one channel in the data set. The power is in linear scale.

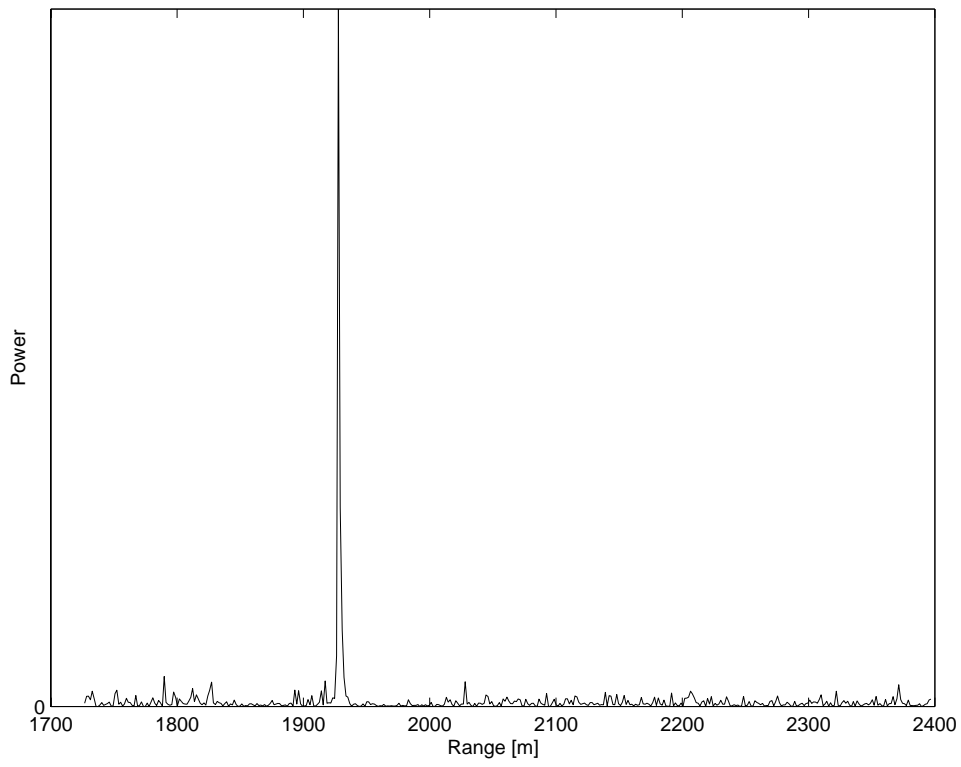


Figure 12. The clutter suppressed sub-aperture beam from Figure 11 after clutter suppression. The clutter suppression is above 20dB. The power is in linear scale.

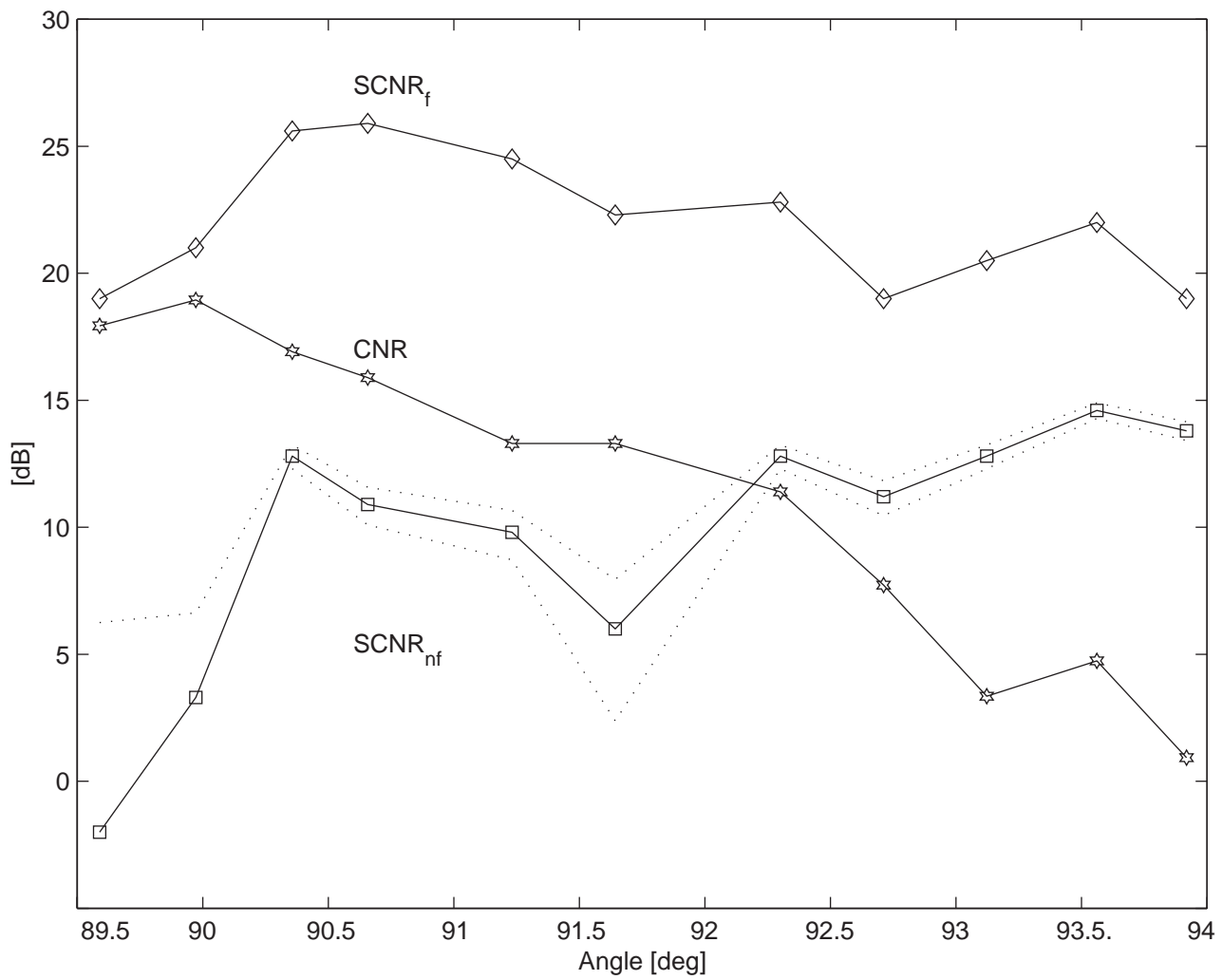


Figure 13. The unknown moving target at range 1750 meters. The three curves are $SCNR_f$, $SCNR_{nf}$ and CNR as a function of Doppler angle. The $SCNR_{nf}$ and $SCNR_f$ are the $SCNR$ before and after clutter suppression has been applied, respectively. The error lines of the $SCNR_{nf}$ estimate is given by the variance and is indicated with dashed lines.

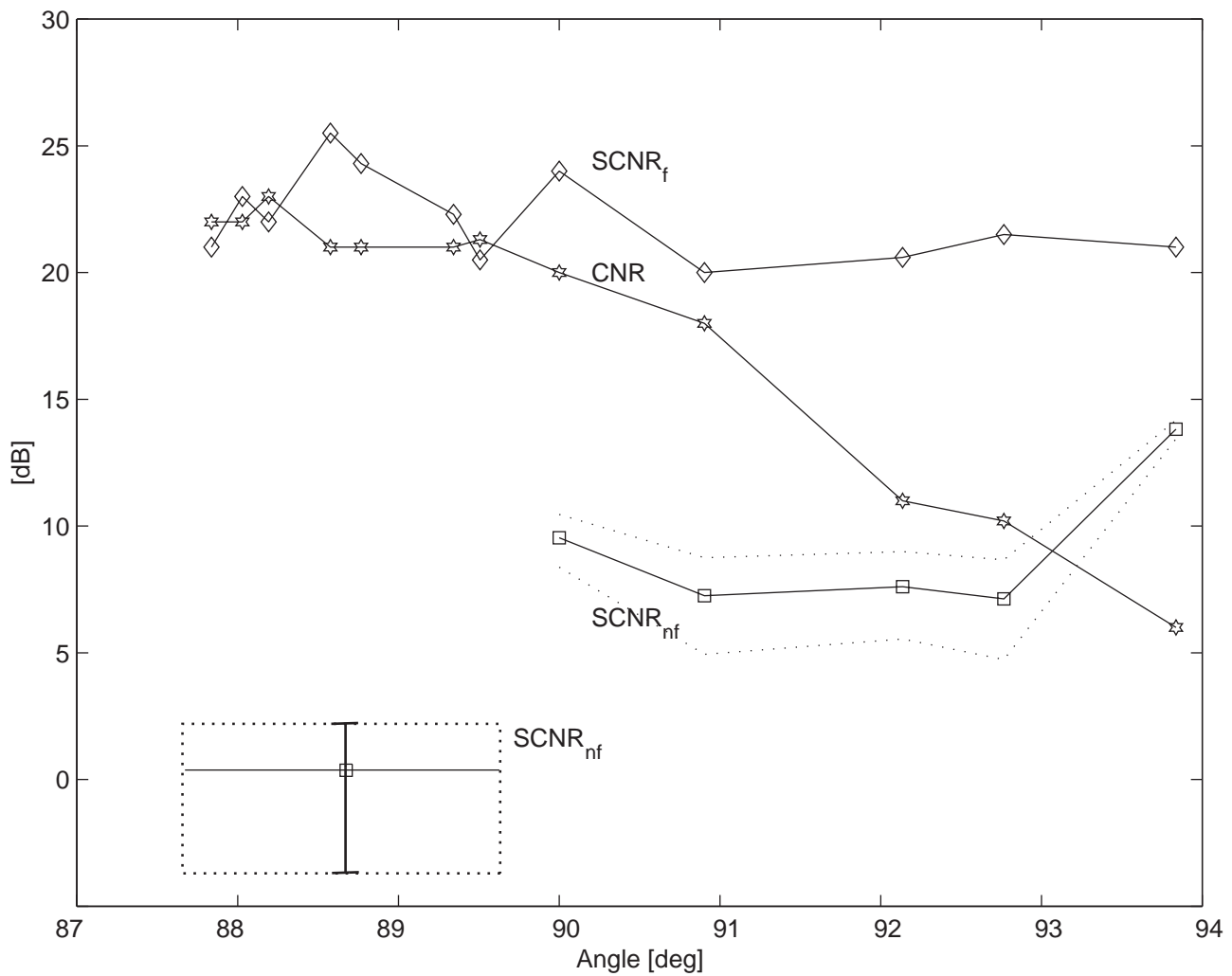


Figure 14. The military moving target at range 1950 meters. The three curves are SCNR_f, SCNR_{nf} and CNR as a function of Doppler angle. SCNR_{nf} and SCNR_f are the SCNR before and after clutter suppression has been applied. The error lines of the SCNR_{nf} estimate is given by the variance and is indicated with dashed lines. Due to the low SCNR_{nf} at low angles seven sub-aperture beams are averaged to provide one SCNR_{nf} estimate, which appears in the dashed box in the lower left-hand corner.